Functionalization Pattern of Graphene Oxide Sheets Controls Entry or Produces Lipid Turmoil in Phospholipid Membranes

Functionalization Pattern of Graphene Oxide Sheets Controls Entry or Produces Lipid Turmoil in Phospholipid Membranes

Marco Dallavalle; Andrea Bottoni; Matteo Calvaresi; Francesco Zerbetto. *ACS Appl. Mater. Interfaces* **2018** *10* (18), 15487-15493
DOI: 10.1021/acsami.8b03224

Publication Date (Web): April 13, 2018
Available at: https://pubs.acs.org/doi/10.1021/acsami.8b03224

The Functionalization Pattern of Graphene Oxide Sheets Controls Entry or Produces Lipid Turmoil in Phospholipid Membranes

Marco Dallavalle,[†] Andrea Bottoni, Matteo Calvaresi, Francesco Zerbetto**

Dipartimento di Chimica "G. Ciamician", Alma Mater Studiorum - Università di Bologna, via F. Selmi 2, 40126 Bologna, Italy

KEYWORDS. Graphene oxide, membranes, phospholipids, nanotoxicity, molecular dynamics, coarse grain modelling

ABSTRACT. Molecular dynamics, coarse-grained to the level of hydrophobic and hydrophilic interactions, shows that graphene oxide sheets, GOS, can pierce through the phospholipid membrane and navigate the double layer only if the hydrophilic groups are randomly dispersed in the structure. Their behavior resembles that found in similar calculations for pristine graphene sheets. If the oxidation is located at the edge of the sheets, GOS hover over the membrane and trigger a major re-organization of the lipids. The re-organization is largest when the radius of the edge-functionalized sheet is similar to the length of the lipophilic chain of the lipid. In the reorganization, the heads of the lipid chains form dynamical structures that pictorially resembles the swirl of water flowing down a drain. All effects maximize the interaction between hydrophobic moieties on the one hand and lipophilic fragments on the other and are

accompanied by a large number of lipid flip-flops. Possible biological consequences are discussed.

INTRODUCTION

Possible short- and long-term adverse health impact of any new material ought to be understood before practical exploitation. This is even more the case when envisaged applications include biomedical and sensing devices, drug delivery, and tissue engineering, as is the case for graphene and related materials.[1-5] In particular, graphene oxide, GO, is a promising platform for a number of applications because of its ease of processability and low cost. For pristine graphene sheets, the reported cytotoxicity was hypothesized to originate from direct interactions between graphene and cell membranes that cause serious physical damages to the membranes. Simulations provided additional information on the interaction between graphene sheets and lipid membranes.[6-12]

In living cells, GO exhibited dose-and size-dependent toxicity.[13] GO exhibited bactericidal properties on several pathogens even at low doses and was suggested as a bactericide for controlling plant diseases.[14-15] *Pseudomonas Putida* in contact with GO lost membrane integrity.[16] GO sheets were also highly effective in inhibiting the growth of dental pathogens by destroying the integrity of their membrane.[17] Synthesized GO showed dose-dependent toxicity to a yeast, *Pichia Pastoris*, through cell membrane damage.[18] In algae, toxic effects of GO were observed at concentrations from 10 $\mu g\ ml^{-1.}$ Such toxicity was ascribed also to membrane damage.[19] Larger GO sheets entrapped single-celled *Chlorella Vulgaris* and reduced cell permeability.[20] Rat basophilic leukemia cells showed profound plasma membrane ruffling and shedding induced by GO.[21] SEM images of bacteria after the exposure to laser irradiated

graphene oxide showed membrane damage.[22] Polyamide membranes were imparted strong antimicrobial properties by GO functionalization.[23] In general, it was found that direct contact of microorganisms and living cells with carbon nanostructures seriously affects their cellular membrane integrity, metabolic processes and morphology.[24] Even in the reduced form, graphene oxide induced cell wall damage and membrane integrity loss.[25] On the contrary, carboxyl functionalized graphene was internalized by cells without causing any toxicity.[26] The presence of wrinkles in GO films increased substantially membrane damage in bacteria.[27] The effect of GO on the morphology, viability, mortality and membrane integrity of A549 cells was considered. The results suggested that GO does not enter the cells and has no obvious cytotoxicity. However, GO can induce loss of cell viability at high concentration.[28] GO can also cause a dose-dependent oxidative stress in living cells and induce loss of cell viability at high concentration.[3] Less oxidized graphenes were the less cytotoxic while larger and more oxidized graphenes were more cytotoxic.[29] GO can affect red blood cells morphology and membrane integrity in a concentration-dependent way.[30] The size of the GO sheet is important. The antimicrobial activity of GO surface coatings increased 4-fold when GO sheet area decreased from 0.65 to 0.01 micron squared. The higher antimicrobial effect of smaller GO sheets is attributed to the higher defect density of smaller sheets.[31] An atomic force microscopy study of GO and *Escherichia coli* showed that the interactions of GO and living cells are weak or predominantly repulsive, with only sporadic adhesion forces.[32] In order to simplify the system, the propensity of GO to attach to and disrupt model cell membranes was studied using supported vesicular layers of zwitterionic 1,2-dioleoyl-sn-glycero-3-phosphocholine. The lipid vesicles were disrupted upon attachment of GO. When the exposure to GO was terminated, the pores of the lipid bilayers were sealed indicating a self-healing ability.[33]

Molecular dynamics simulations showed that the graphene sheets can be inserted in biological membranes.[8] Local piercing by sharp protrusions initiates membrane penetration.[6] For larger nanosheets, coarse-grained simulations showed that the translocation entails a vesiculation process.[9] Another study demonstrated that edge oxidized graphene nanosheets can pierce the bilayer to reach the center of the bilayer or stand upwards across the bilayer, depending on the degree of oxidation.[10] Graphenes covered by a low density of lipid molecules can still pierce into the bilayer.[10] Piercing is hindered if the whole body of graphene is fully encapsulated in a lipid micelle.[10] Detailed translocation pathways of these materials across the cellular membrane was obtained together with a phase diagram in the space of oxidization degree and particle size.[11] A hemispheric vesicle superstructure was formed through the adhesion of graphene to the top surface of the membrane.[11] Further molecular dynamics simulations showed that when graphene oxide is embedded in the membrane, several lipids are pulled out of the membrane to the surface of GO, resulting in pore formation and water molecules flowing into the membrane.[34]

Crucially, the toxicity of GOS is not matched by other 2D materials. In a comparative study, nanoclay particles exhibited very low or no toxicity towards *Paramecium Caudatum*, whereas graphene oxide was toxic.[35]

In this scenario, it appears that GO sheets induce or do not induce loss of membrane viability and the effects are strongly dependent on the size of the sheet. It is therefore of interest to identify the driving forces for the interactions between GO sheets and lipid membranes.[36-40] In order to achieve a deeper understanding, we decided to use a protocol that we have developed before to investigate the interactions of graphene sheets with the phospholipid membrane.[41] The protocol exploits repeated molecular dynamics simulations that allow reaching statistical significance.[41] It showed before that graphene sheets, when sufficiently large, adsorb on the top

of the phospholipid membrane and make the chains somersault so that their hydrophobic fragment is in contact with the hydrophobic graphene sheet. [41]

In this work, we focus on some unexplored effects of GO sheets of increasing size and different hydrophilic functionalization on the structure of the phospholipid bilayer. Pristine graphene is insoluble, a feature that hinders technological application. Basal-plane-functionalization, via chemical grafting or noncovalent adsorption, has been exploited for preparing solution-processable graphene sheets.[42] Alternatively, edge-functionalization is of interest since the dangling bonds at the edge of a graphene sheet are more reactive than the carbon atoms of the basal plane. Edge-functionalization preserves basal plane integrity,[43] makes edge-functionalized graphene (ef-GOS) dispersable and processable, and ultimately retains the physicochemical properties of the pristine graphene.

COMPUTATIONAL DETAILS

The DPD model used in this work is based on the approach introduced by Groot and coworkers.[44,45] The equations of motion are integrated using a modified velocity–Verlet algorithm.[44] All calculations were carried out using the suite of programs Culgi 4.0.[46]

The parameters

In this study, a phospholipid molecule consists of three linearly connected hydrophilic beads (labeled with the letter H), representing the polar head-group, to which two tails of six hydrophobic beads (labeled by the letter T) are jointed. The water particle is labeled by the letter W. The GOS is modeled as an aggregate of beads (labeled by the letter G), as originally proposed by Koelman and Hoogerbrugge.[47]

The interactions between any two particles in the solution are described by the parameters in Table 1. The parameters for the phospholipids were taken from the well-validated model of Shillcock and Lipowsky[48] that is capable of reproducing the structural properties and the stress profile of bilayers. The stretch modulus and the bending rigidity of the membrane simulated with these parameters are comparable to experimental values for typical phospholipid bilayers. For the interaction between graphene and phospholipids we used a set of parameters developed to reproduce the experimental self-assembly of carbon nanomaterials with amphiphilic molecules.[41,49-52] An additional validation of these parameters is showed in the SI.

In the simulations, the bead density was set at $\rho = 3$. A cubic simulation box of dimension 32 r_c x 32 r_c x 32 r_c was used and periodic boundary conditions were applied.

The total number of beads was 98,304. Each of the calculations was run for 2,500,000 steps using a time step of 0.05τ.

Table 1. Parameters for bead pair interactions. Conservative force parameter a_{ij} in units of k_BT/r_c. H = Head-group bead, hydrophilic bead on Graphene; T = Tail bead; W = Water bead; G = Graphenoid bead.

a_{ij}	**H**	**T**	**W**	**G**
H	25	50	35	50
T	50	25	75	30
W	35	75	25	75
G	50	30	75	25

Phospolipids are constructed by tying beads together using Hook springs with the potential $U_2(i, i+1) = 1/2\ k_2 (\ | r_{i,i+1} | - l_0\ )^2$ where i, i+1 represents adjacent beads in the phospolipids.[48] The spring constant, k_2, and unstretched length, l_0, are chosen so as to fix the average bond

length to a desired value (see Table 2).[48] Both parameters may be specified independently for each bead pair. Chain stiffness is modeled by a three-body potential acting between three adjacent beads in a chain, $U_3(\text{i-1,i,i+1}) = k_3[\ 1\text{-cos}\ (\Phi - \Phi_0)\ ]$ where the angle Φ is defined by the scalar product of the two bonds connecting beads i-1, i, and i, i+1. [48] The bending constant, k_3, and preferred angle, Φ_0, may be specified independently for different bead triplets. [48]

Table 2. Bond and angle parameters.

Bond Pair	k_2	l_0
H H	128	0.5
H T	128	0.5
T T	128	0.5
Bead Triplets	k_3	Φ_0
T T T	20	180
H T T	20	180

Simulated System and Physical Length and Time Scales. For transformation of dimensionless time units into physical length and time scales, it is necessary to link simulations with experimental data. The center-center distance between polar head group (PH) layers in cellular membranes is typically in the range of 40 Å (30 Å hydrophobic core (HC) domain, plus 5+5 Å for each half of the PH domain). In the simulations this value corresponds to 6.955 r_c, where r_c is the unit length in the system. From the above equivalence we determine r_c = 5.75 Å.

Following Groot and Rabone[53] the physical time scale may be obtained from a comparison of the calculated diffusion constant of water beads, D_{calc} to the experimental value[54] D_{exp} = 2.43 10^{-5} cm^2/s

$$t = \frac{N_m D_{calc} r_c^2}{D_{exp}}$$

N_m is the number of water molecules forming a "water bead" and the estimated self-volume for a single water molecule is 30 Å^3. Since a cubic volume of size r_c^3 (190.1 Å^3) represents ρN_m water molecules, with ρ=3 being the number of beads per cubic r_c^3 it follows that N_m = 2.1.

In the simulations, the diffusivity of a particle is a dimensionless parameter that characterizes the fluid. It may be regarded as the ratio between the time needed by the particle to diffuse out to a certain distance and the time necessary for the hydrodynamic interactions to reach steady state conditions over comparable distances.[44] The diffusion coefficient of each bead is obtained by calculating the mean square displacement according to[53]

$$D = \lim_{t\to\infty} \frac{1}{6t} \left\langle \left| r_i(t) - r_i(t=0) \right|^2 \right\rangle$$

The resulting value of D_{calc} = 0.31 substituted into the above equation yields a final time unit of 88.6 ps. The simulation length corresponds to a physical time of 11 μs.

RESULTS AND DISCUSSION

The simulations were carried out using Dissipative Particle Dynamics, DPD, that has found a large variety of applications in the investigation of materials and interfaces.[55-64] Figure 1 shows the models of the moieties used in the simulations. Edge functionalization was simulated by changing all the hydrophobic beads located at the border of the graphene flake into hydrophilic ones.[41] Random functionalization was simulated by replacing randomly some of the hydrophobic beads of the graphene flake (both in the basal plane and at the edges) in hydrophilic beads.[41] The

hydrophilic beads are 30%, a value close to the oxygen content in GO. Edge functionalized GOS are labeled ef-GOS; randomly functionalized GOS are labeled rf-GOS.

Simulations were repeated five times from different initial positions of the sheets in order to acquire sufficient statistics.

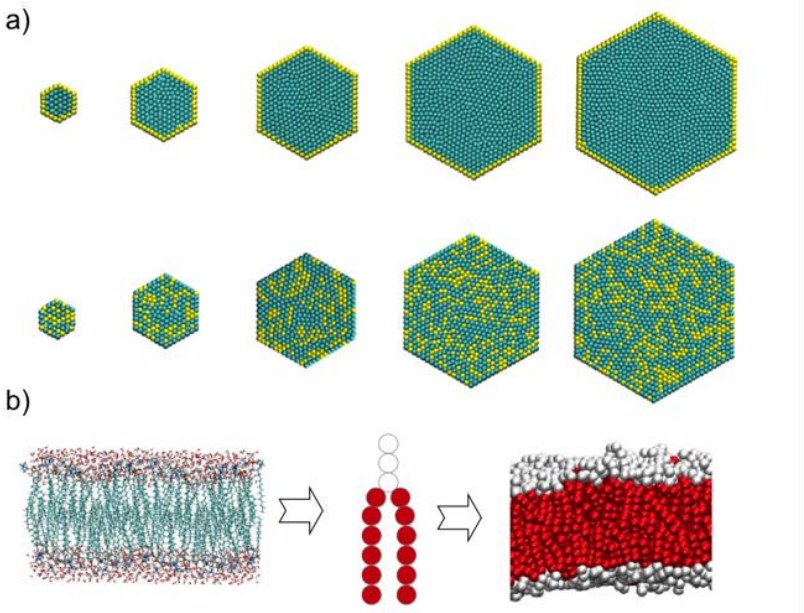

Figure 1. Description of coarse-grained molecular dynamics models: a) Coarse graining of the graphene oxide sheets. (Top) Edge functionalized GOS, ef-GOS; (Bottom) randomly functionalized GOS, rf-GOS. Petroleum blue hydrophobic beads of GO, yellow hydrophilic beads of GO. From left to right, the sizes are 2.7 nm, 5.2 nm, 8.1 nm, 11.2 nm, 13.3 nm. The size of the flakes was obtained by converting the dimensionless physical length of the flakes with the conversion factor r_c = 5.75 Å, determined as explained in the "Simulated System and Physical Length and Time Scales" section. b) Coarse graining of the membrane. On the right side representation of the lipids: red hydrophobic beads, white hydrophilic.

Figure 2 provides snapshots of the systems at the end of one of the 11 microsecond simulations. The functionalization pattern of the GOS determines its final configuration with

respect to the bilayer. Only rf-GOS pierce through the membrane, while ef-GOS hover over and adhere to the membrane.

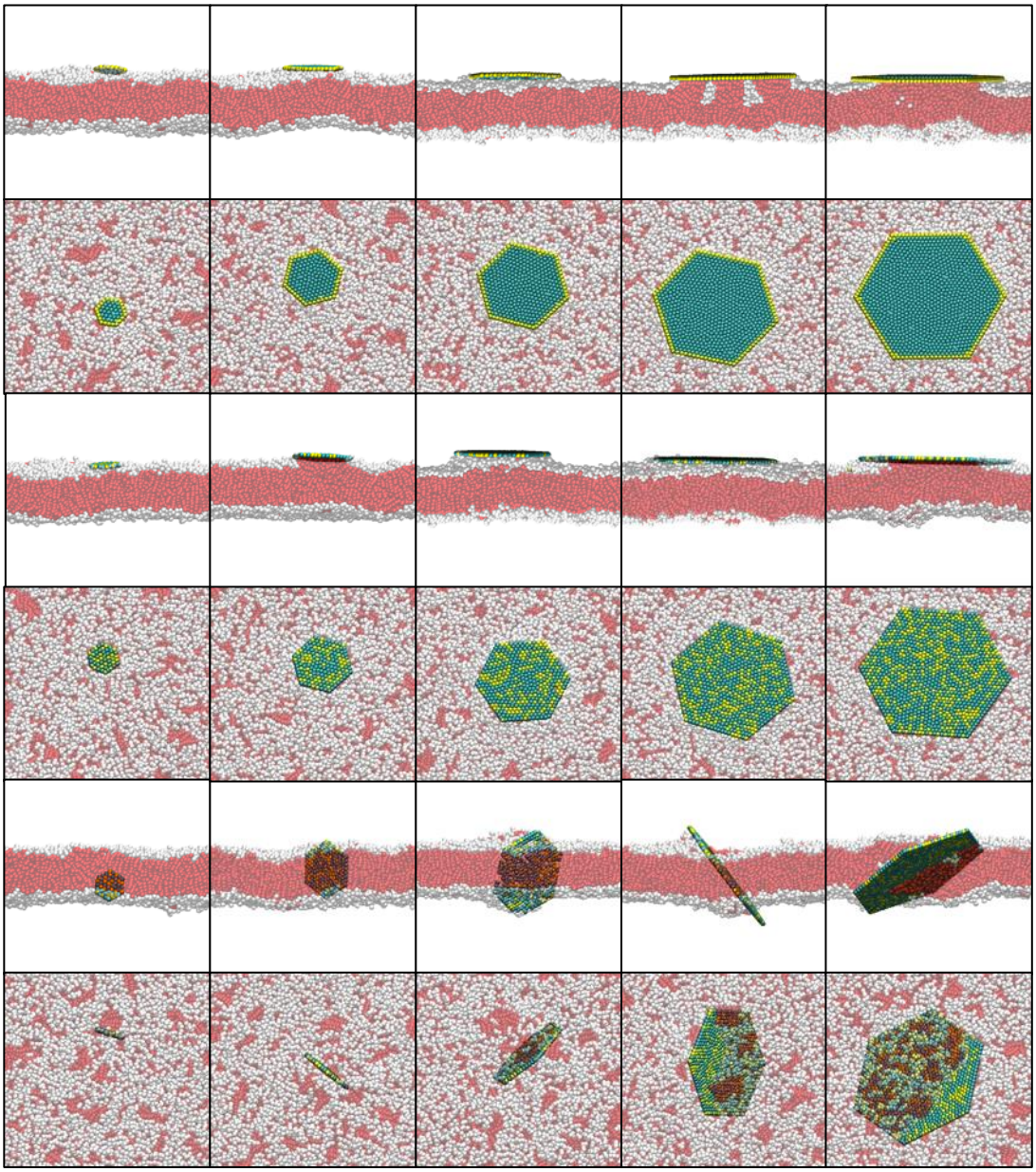

Figure 2. Illustrative snapshots, at the end of the simulations, of GOS of increasing size with two different functionalization patterns. From left to right, sizes of 2.7 nm, 5.2 nm, 8.1 nm, 11.2 nm, 13.3 nm. White: hydrophilic heads of the phospholipids; red: hydrophobic phospholipid tails;

petroleum blue: hydrophobic graphene beads, yellow: hydrophilic graphene beads. For clarity, water is not shown. Top and bottom pairs of rows are different perspectives of the sheets.

In previous simulations,[41] pristine graphene sheets, smaller than 5.2 nm, were found to navigate inside the membrane. Increasing their size up to 11.2 nm, the sheets crossed the bilayer only when a suitable geometric orientation was met, and two entirely different stable structures were found in the free energy surface. In the first one, the sheet pierced through, in the second one it adsorbs onto the membrane. If larger than 11.2 nm, the sheets were unable to cross the membrane. These results confirmed experimental and computational data of size-dependency on graphene sheets cellular internalization process.[11,65-67]

The behavior of rf-GOS is somewhat similar to that of GS, but they can pierce through the membrane regardless of their size, while ef-GOS consistently behave as larger GS and never enter the bilayer.

In figure 3, the x-axis shows the angle formed by the sheet with the phospholipid bilayer. A value of the angle close to 0˚ means that the sheet is parallel to the membrane; a value close to 90˚ means that it is perpendicular to it. The y-axis is the distance of the center of mass of the sheet from the ideal surface that separates the two layers of phospholipids.

The different behavior of the two types of functionalization is apparent. In the case of the ef-GOs, the minimum of the free energy is consistently found with the sheets lying on the lipid surface. As the size of the sheet increases, the minimum becomes tighter and tighter and exists only for truly flat-lying sheets that are sprawled out like a bear skin rug. For smaller ef-sheets, the free energy minimum is wider, which implies greater mobility of the sheet. In the case of the

rf-GOs, alongside the “bear skin rug” minimum, there is a secondary but still populated minimum where the rf-GOs penetrates the membrane.

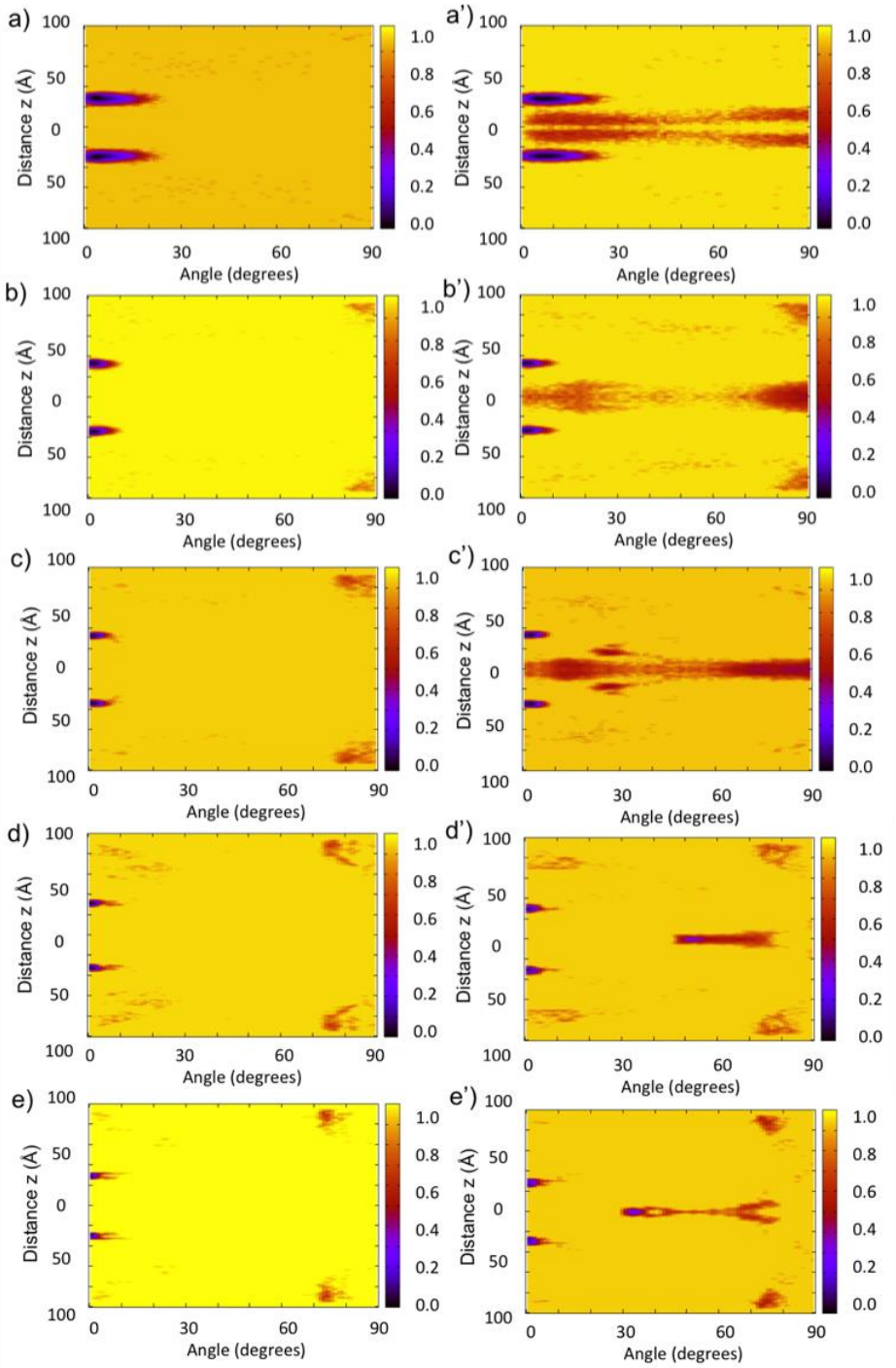

Figure 3. Normalized free energy as a function of the penetration and orientation of the sheet. Sizes: (a) and (a') 2.7, (b) and (b)' 5.2, (c) and (c)' 8.1, (d) and (d') 11.2, (e) and (e') 13.3 nm. Left (a) to (e): ef-GOS; right (a') to (e'): rf-GOS

The adsorption of pristine graphene flakes triggered translocations from one layer to the other of multiple phospholipids. The majority of translocation events occurred as soon as the graphene sheet settled on the top of the layer in less than a microsecond. The re-organization was truly related to the hydrophobic-hydrophobic interaction that allowed the sheet to adhere to the membrane. Table 3 shows the number of flip-flops as a function of the size of the GOS and its functionalization. The reference number in the absence of any carbon sheet for simulations of the same length is 3.

Table 3. Average number, over five dynamics, of flip-flops during 11 microseconds of dynamics for different sheets sizes. An unperturbed membrane is characterized by an average number of 3 translocation events.

Nanosheet size (nm)	Number of translocation events for graphene sheets	Number of translocation events for border functionalized graphene oxide sheets	Number of translocation events for randomly functionalized graphene oxide sheets
2.7	4	8	9
5.2	8	65	40
8.1	17	30	21
11.2	41	36	25
13.3	46	39	41

It is apparent that introduction of hydrophilic fragments increases the number of lipid translocations with respect to pristine graphene. The distribution of the displacement has a local maximum for small sheets of 5.2 nm. In particular, ef-GOS are extremely efficient at promoting migration of lipids from one layer to the other.

The issue arises of the origin of the increased number of flip-flops and their possible consequences. Figure 4 shows the effect of the increased number of flip-flops for small size ef-GOS.

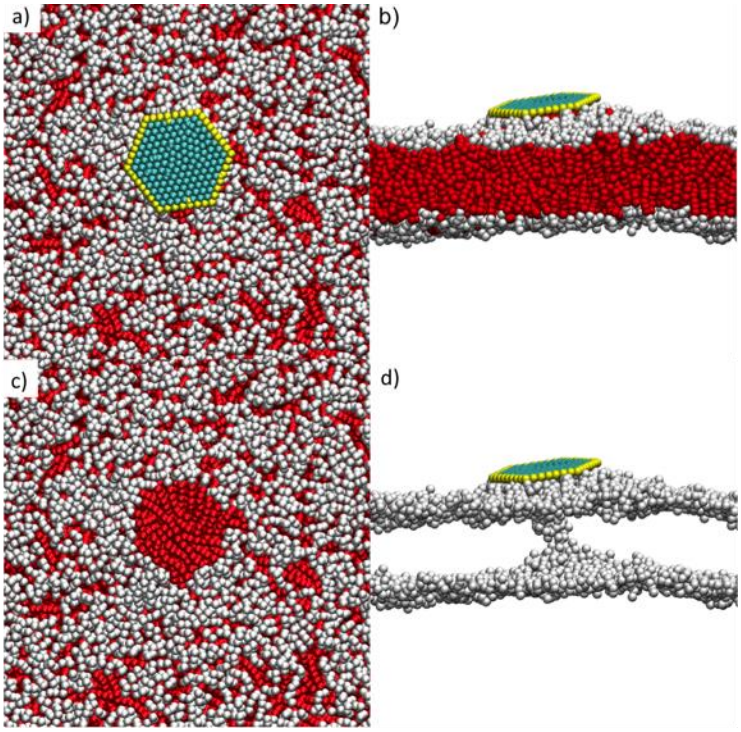

Figure 4. a) Top view and b) side view of a ef-GOS of 5.2 nm adhering to the phospholipid membrane. c) Peeling off the sheet shows that the hydrophobic tails directly interact with hydrophobic basal plane of ef-GOS and the hydrophilic functionalization attracts the lipid heads. d) Formation of a phospholipid swirl in the membrane induced by ef-GOS adhesion. For sake of clarity, on the right, only the lipids heads of the phospholipids are shown.

A dynamical swirl of lipid heads forms beneath the GOS. The hydrophilic beads can form a stabilizing interaction with the phospholipid heads. The heads re-organize their position to maximize the interaction. Edge functionalization introduces order in the interaction for two reasons (Figure 4b): on the one hand the hydrophilic beads of ef-GOS attract the lipid heads, on the other hand, the hydrophobic chain can adsorb on the lipophylic surface of the ef-GOS. When the diameter of the ef-GOS is twice the length of the lipid, a third cause of order is introduced since the lipids can arrange radially from the center of the sheet to form a bike wheel-like structure (Figure 4d). This *structure* cannot be sustained throughout the membrane. Indeed, the bottom layer of the membrane has to retain as much as possible its lipophilic and hydrophilic interactions. In order to do this, the lipids re-organize and the wheel-like structure tapers off. The net effect is that the heads form a swirl inside the membrane.

As in the case of pristine graphene,[41] the presence of the sheet may affect the overall density distribution of the hydrophobic and hydrophilic moieties of the phospholipids. Figure 5 compares the densities for the perturbed bilayer when the GOS pierced through or adhered to the membrane. Random functionalization introduces an asymmetry in the distribution of water, and both heads and tails of the lipids.

A small GOS penetrating the membrane does not affect the overall density distribution of the hydrophobic and hydrophilic moieties of the phospholipids, which resembles the distribution of an unperturbated membrane. When a large flake penetrates the membrane, some phospholipids stick to the GOS and follow its movements. The head beads are no longer excluded from the bilayer interior and the two monolayers are no longer properly organized.

When GOS adsorbs on the membrane, an asymmetry appears in the membrane bilayer because the hydrophobic tails tend to move toward the interface with the GOS as described in the previous paragraph. This effect is size dependent.

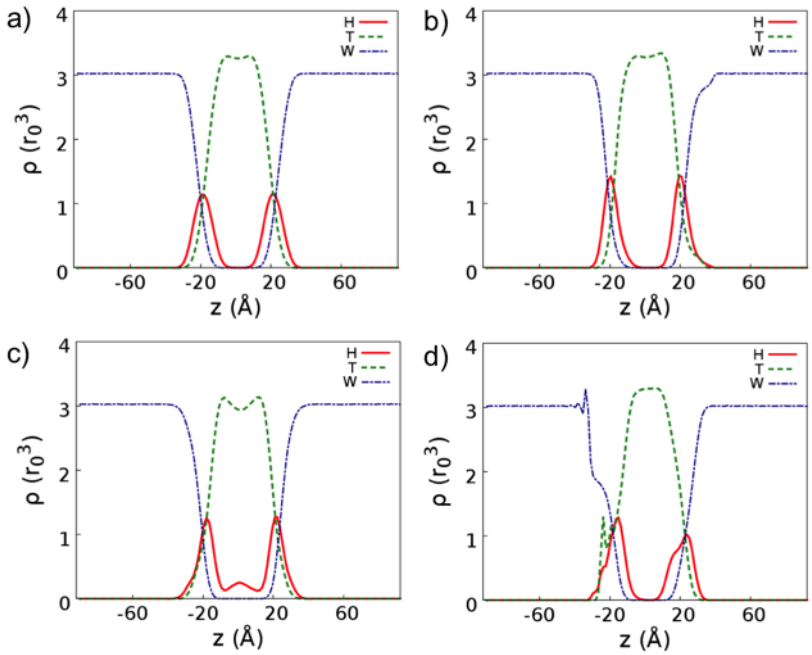

Figure 5. Density profiles of the phospholipid bilayers. Hydrophilic head beads, H; hydrophobic tail beads, T; bulk water, W. a) rf-GOS of 5.2 nm piercing the membrane; b) ef-GOS of 5.2 nm adhering to the membrane; c) rf-GOS of 13.3 nm piercing the membrane; d) ef-GOS of 13.3 nm adhering to the membrane. The profiles were averaged over 1000 steps.

Biologically, phospholipids re-organization in the cellular membrane can trigger a number of events, including recognition and elimination of apoptotic or aged cells.[68] GOS piercing through the membrane may impair cell functioning through disruption of the membrane proteins location and 3D spatial arrangement, while GOS adhesion can modify the polarization of the cellular membrane and eventually induce cytotoxicity.

CONCLUSION

Graphene and graphene oxides sheets can affect strongly cellular viability. The antibacterial properties of GOS have been proved experimentally a number of times. The present simulations show that structurally different sheets of graphene oxides interact with the cellular membrane in a qualitatively different way with respect to sheets of pristine graphene. GS navigate the membrane when small and adhere to it when large, thereby flipping the lipids underneath them. Randomly functionalized GOS still penetrate the membrane when their size is substantially greater than that of GS that only adhere to it. The random functionalization therefore improves flakes penetration. Edge functionalized GOS always lie on top of the lipid bilayer, confirming the importance of the edges in controlling the sheet penetration. Ef-GOS increase the masking effect of the graphene flakes; in particular, small ef-GOS profoundly re-organize the phospholipid bilayer. Commensurability of a hydrophilic perimeter with the lipid chain length drives the re-organization. In other words, the formation of a swirl-like structure made by heads of lipids is triggered by the presence of an oxidation pattern where lipids can arrange with their polar heads on a hydrophilic moiety of the edge of the GOS, while their tails touch each other. These hydrophilic patterns can exist also as a local decoration of larger sheets.

The effect that arises with the commensurability of a hydrophilic perimeter in GOS with the lipid chain length can also be exploited for fabricating new lipid structures and promote new patterns of lipid self-assembly.

SUPPORTING INFORMATION

The Supporting Information is available free of charge on the ACS Publications website. Validation of the interaction parameters used in the simulations.

AUTHOR INFORMATION

Corresponding Author

Phone: +39-051-2099473. E-mail: francesco.zerbetto@unibo.it (F.Z.)

Phone: +39-051-2099478. E-mail: matteo.calvaresi3@unibo.it (M. C.)

Present Addresses

† Eduard-Zintl-Institut für Anorganische und Physikalische Chemie, Center of Smart Interfaces, Technische Universität Darmstadt, Germany

ACKNOWLEDGMENT

This project has received funding from the European Union's Horizon 2020 research and innovation programme under grant agreement No 696656 (Graphene Flagship)

REFERENCES

1. Kostarelos, K.; Novoselov, K. S. Exploring the Interface of Graphene and Biology. *Science* **2014***, 344*, 261-263.

2. Feng, L.; Liu, Z. Graphene in Biomedicine: Opportunities and Challenges. *Nanomedicine*, **2011**, *6*, 317-324.

3. Sanchez, V. C.; Jachak, A.; Hurt, R. H.; Kane, A. B. Biological Interactions of Graphene-Family Nanomaterials: An Interdisciplinary Review. *Chem. Res. Toxicol.* **2012**, 25, 15-34.

4. Nguyen, P.; Berry, V. Graphene Interfaced with Biological Cells: Opportunities and Challenges. *J. Phys. Chem. Lett.* **2012**, *3*, 1024-1029.

5. Zhang, Y.; Nayak, T. R.; Hong, H.; Cai, W. B. Graphene: A Versatile Nanoplatform for Biomedical Applications. *Nanoscale* **2012**, *4*, 3833-3842.

6. Li, Y.; Yuan, H.; Von dem Bussche, A.; Creighton, M.; Hurt, R. H.; Kane, A. B.; Gao, H. Graphene Microsheets Enter Cells Through Spontaneous Membrane Penetration at Edge Asperities and Corner Sites. *Proc. Natl. Acad. Sci. U.S.A.* **2013**, *110*, 12295-12300.

7. Tu, Y.; Lv, M.; Xiu, P.; Huynh, T.; Zhang, M.; Castelli, M.; Liu, Z.; Huang, Q.; Fan, C.H.; Fang, H.P.; Zhou, R.H. Destructive Extraction of Phospholipids from *Escherichia coli* Membranes by Graphene Nanosheets. *Nat. Nanotechnol.* **2013**, *8*, 594-601.

8. Titov, A. V.; Kral, P.; Pearson, R. Sandwiched Graphene-Membrane Superstructures. *ACS Nano* **2010**, *4*, 229-234.

9. Guo, R.; Mao, J.; Yan, L.-T. Computer Simulation of Cell Entry of Graphene Nanosheet. *Biomaterials* **2013**, *34*, 4296-4301.

10. Wang, J.; Wei, Y.; Shi, X.; Gao, H. Cellular Entry of Graphene Nanosheets: The Role of Thickness, Oxidation and Surface Adsorption. *RSC Adv.* **2013**, *3*, 15776-15782.

11. Mao, J.; Guo, R.; Yan, L.-T. Simulation and Analysis of Cellular Internalization Pathways and Membrane Perturbation for Graphene Nanosheets. *Biomaterials* **2014**, *35*, 6069-6077.

12. Chen, P.; Yan, L.-T. Physical Principles of Graphene Cellular Interactions: Computational and Theoretical Accounts. *J. Mater. Chem. B* **2017**, *5*, 4290-4306.

13. Cho, Y. C.; Pak, P. J.; Joo, Y. H.; Lee, H. S.; Chung, N. *In Vitro* and *in Vivo* Comparison of the Immunotoxicity of Single- and Multi-layered Graphene Oxides with or Without Pluronic F-127. *Sci. Rep.* **2016**, *6*, 38884.

14. Chen, J. N.; Wang, X. P.; Han, H. Y. A New Function of Graphene Oxide Emerges: Inactivating Phytopathogenic Bacterium *Xanthomonas Oryzae pv. Oryzae*. *J. Nanopart. Res.* **2013**, *15*, 1658.

15. Chen, J. N.; Peng, H.; Wang, X. P.; Shao, F.; Yuan, Z. D.; Han, H. Y. Graphene Oxide Exhibits Broad-Spectrum Antimicrobial Activity Against Bacterial Phytopathogens and Fungal Conidia by Intertwining and Membrane Perturbation. *Nanoscale* **2014**, *6*, 1879-1889.

16. Combarros, R. G.; Collado, S.; Diaz, M. Toxicity of Graphene Oxide on Growth and Metabolism of *Pseudomonas Putida*. *J. Hazard. Mater.* **2016**, *310*, 246-252.

17. He, J. L. ; Zhu, X. D.; Qi, Z. N. ; Wang, C.; Mao, X. J.; Zhu, C. L. ; He, Z. Y. ; Lo, M. Y.; Tang, Z. S. Killing Dental Pathogens Using Antibacterial Graphene Oxide. *ACS Appl. Mater. Interfaces* **2015**, *7*, 5605-5611.

18. Zhang, M.; Yu, Q.; Liang, C.; Liu, Z.; Zhang, B.; Li, M. C. Graphene Oxide Induces Plasma Membrane Damage, Reactive Oxygen Species Accumulation and Fatty Acid Profiles Change in *Pichia Pastoris*. *Ecotoxicol. Environ. Saf.* **2016**, *132*, 372-378.

19. Nogueira, P. F. M.; Nakabayashi, D. ; Zucolotto, V. The Effects of Graphene Oxide on Green Algae *Raphidocelis Subcapitata*. *Aquat. Toxicol.* **2015**, *166*, 29-35.

20. Ouyang, S. H.; Hu, X. G.; Zhou, Q. X. Envelopment-Internalization Synergistic Effects and Metabolic Mechanisms of Graphene Oxide on Single-Cell *Chlorella Vulgaris* Are Dependent on the Nanomaterial Particle Size. *ACS Appl. Mater. Interfaces* **2015**, *7*, 18104-18112.

21. Sun, C.; Wakefield, D. L.; Han, Y. M.; Muller, D. A. ; Holowka, D. A.; Baird, B. A.; Dichtel, W. R. Graphene Oxide Nanosheets Stimulate Ruffling and Shedding of Mammalian Cell Plasma Membranes. *Chem.* **2016**, *1*, 273-286.

22. Buccheri, M. A.; D'Angelo, D.; Scalese, S.; Spano, S. F.; Filice, S.; Fazio, E.; Compagnini, G.; Zimbone, M.; Brundo, M. V.; Pecoraro, R.; Alba, A.; Sinatra, F.; Rappazzo, G.; Privitera, V. Modification of Graphene Oxide by Laser Irradiation: A New Route to Enhance Antibacterial Activity. *Nanotechnology* **2016**, *27*, 245704.

23. Perreault, F.; Tousley, M. E.; Elimelech, M. Thin-Film Composite Polyamide Membranes Functionalized with Biocidal Graphene Oxide Nanosheets. *Environ. Sci. Technol. Lett.* **2014**, *1* 71-76.

24. Dizaj, S. M. ; Mennati, A. ; Jafari, S. ; Khezri, K.; Adibkia, K. Antimicrobial Activity of Carbon-Based Nanoparticles. *Adv. Pharm. Bull.* **2015**, *5*, 19-23.

25. Du, S. T.; Zhang, P.; Zhang, R. R.; Lu, Q.; Liu, L.; Bao, X. W.; Liu, H. J. Reduced Graphene Oxide Induces Cytotoxicity and Inhibits Photosynthetic Performance of the Green Alga *Scenedesmus Obliquus*. *Chemosphere* **2016**, *164*, 499-507.

26. Sasidharan, A.; Panchakarla, L. S.; Chandran, P.; Menon, D.; Nair, S.; Rao, C. N. R.; Koyakutty, M. Differential Nano-Bio Interactions and Toxicity Effects of Pristine Versus Functionalized Graphene. *Nanoscale* **2011**, *3*, 2461-2464.

27. Zou, F. M.; Zhou, H. J.; Jeong, D. Y.; Kwon, J.; Eom, S. U.; Park, T. J.; Hong, S. W.; Lee, J. Wrinkled Surface-Mediated Antibacterial Activity of Graphene Oxide Nanosheets. *ACS Appl. Mater. Interfaces.* **2017**, *9*, 1343-1351.

28. Chang, Y. L.; Yang, S. T. ; Liu, J. H.; Dong, E.; Wang, Y. W.; Cao, A. N. ; Liu, Y. F.; Wang, H. F. *In Vitro* Toxicity Evaluation of Graphene Oxide on A549 Cells. *Toxicol. Lett.* **2011**, *200*, 201-210.

29. Pelin, M.; Fusco, L.; Leon, V.; Martin, C.; Criado, A.; Sosa, S.; Vazquez, E.; Tubaro, A.; Prato, M. Differential Cytotoxic Effects of Graphene and Graphene Oxide on Skin Keratinocytes. *Sci. Rep.* **2017**, *7*, 40572.

30. Feng, R.; Yu, Y. P.; Shen, C. X.; Jiao, Y. P.; Zhou, C. R. Impact of Graphene Oxide on the Structure and Function of Important Multiple Blood Components by a Dose-Dependent Pattern. *J. Biomed. Mater. Res.* **2015**, *103*, 2006-2014.

31. Perreault, F.; de Faria, A. F.; Nejati, S.; Elimelech, M. Antimicrobial Properties of Graphene Oxide Nanosheets: Why Size Matters. *ACS Nano* **2015**, *9*, 7226-7236.

32. Castrillon, S. R. V.; Perreault, F.; de Faria, A. F.; Elimelech, M. Interaction of Graphene Oxide with Bacterial Cell Membranes: Insights from Force Spectroscopy. *Environ. Sci. Technol. Lett.* **2015**, *2*, 112-117.

33. Liu, X. T.; Chen, K. L. Interactions of Graphene Oxide with Model Cell Membranes: Probing Nanoparticle Attachment and Lipid Bilayer Disruption. *Langmuir* **2015**, 31, 12076-12086.

34. Chen, J.L.; Zhou, G.Q.; Chen, L.; Wang, Y.; Wang, X. G.; Zeng, S.W. Interaction of Graphene and its Oxide with Lipid Membrane: A Molecular Dynamics Simulation Study. *J. Phys. Chem. C* **2016**, *120*, 6225-6231.

35. Kryuchkova, M.; Danilushkina, A.; Lvov, Y.; Fakhrullin, R. Evaluation of Toxicity of Nanoclays and Graphene Oxide *in Vivo*: *A Paramecium Caudatum* Study. *Environ. Sci.: Nano* **2016**, *3*, 442-452.

36. Szunerits, S.; Boukherroub, R. Antibacterial Activity of Graphene-Based Materials. *J. Mater. Chem. B*, **2016**, *4*, 6892-6912.

37. Cheng, C.; Li, S.; Thomas, A.; Kotov, N. A.; Haag, R. Functional Graphene Nanomaterials Based Architectures: Biointeractions, Fabrications, and Emerging Biological Applications. *Chem. Rev.* **2017**, *117*, 1826−1914.

38. Tegou, E.; Magana, M.; Katsogridaki, A. E.; Ioannidis, A.; Raptis, V.; Jordan, S.; Chatzipanagiotou, S.; Chatzandroulis, S.; Ornelas, C.; Tegos, G. P. Terms of Endearment: Bacteria Meet Graphene Nanosurfaces. *Biomaterials* **2016**, 89, 38-55.

39. Hegab, H. M.; ElMekawy, A.; Zou, L.; Mulcahy, D.; Saint, C. P.; Ginic-Markovic, M. The Controversial Antibacterial Activity of Graphene-Based Materials. *Carbon* **2016**, *105*, 362-376.

40. Zou, X.; Zhang, L.; Wang, Z.; Luo, Y. Mechanisms of the Antimicrobial Activities of Graphene Materials. *J. Am. Chem. Soc.* **2016**, *138*, 2064-2077.

41. Dallavalle, M.; Calvaresi, M.; Bottoni, A.; Melle-Franco, M.; Zerbetto, F. Graphene Can Wreak Havoc with Cell Membranes. *ACS Appl. Mater. Interfaces*, **2015**, *7*, 4406-4414.

42. Quintana, M.; Vazquez, E.; Prato, M. Organic Functionalization of Graphene in Dispersions. *Acc. Chem. Res.*, **2013**, *46*, 138-148.

43. Quintana, M.; Montellano, A.; del Rio, A. E.; Van Tendeloo, G.; Bittencourt, C.; Prato, M. Selective Organic Functionalization of Graphene Bulk or Graphene Edges. *Chem. Commun.* **2011**, *47*, 9330-9332.

44. Groot, R. D.; Warren, P. B. Dissipative Particle Dynamics: Bridging the Gap Between Atomistic and Mesoscopic Simulation *J. Chem. Phys.* **1997**, *107*, 4423-4435.

45. Groot, R. D.; Madden, T. J. Dynamic Simulation of Diblock Copolymer Microphase Separation. *J. Chem. Phys.* **1998**, *108*, 8713-8724.

46. Culgi BV. The Netherlands. Available from: http://www.culgi.com; **2011**.

47. Koelman, J. M. V. A.; Hoogerbrugge, P. J. Dynamic Simulation of Hard Sphere Suspensions Under Steady Shear. *Europhys. Lett.* **1993**, *21*, 363-368.

48. Shillcock, J. C.; Lipowsky, R. Equilibrium Structure and Lateral Stress Distribution of Amphiphilic Bilayers from Dissipative Particle Dynamics Simulations. *J. Chem. Phys*. **2002**, *117*, 5048-5061.

49. Calvaresi, M.; Dallavalle, M.; Zerbetto F. Wrapping Nanotubes with Micelles, Hemimicelles, and Cylindrical Micelles. *Small* **2009**, *5*, 2191-2198.

50. Höfinger, S.; Melle-Franco, M.; Gallo, T.; Cantelli, A.; Calvaresi, M.; Gomes, J. A. N. F.; Zerbetto, F. A Computational Analysis of the Insertion of Carbon Nanotubes into Cellular Membranes. *Biomaterials* **2011**, *32*, 7079-7085.

51. Min, S. H.; Lee, C.; Jang, J. Dissipative Particle Dynamics Modeling of a Graphene Nanosheet and its Self-Assembly with Surfactant Molecules. *Soft Matter* **2012**, *8*, 8735-8742.

52. Dallavalle, M.; Leonzio, M.; Calvaresi, M.; Zerbetto, F. Explaining Fullerene Dispersion by using Micellar Solutions. *ChemPhysChem* **2014**, *15*, 2998-3005.

53. Groot, R. D.; Rabone, K. L. Mesoscopic Simulation of Cell Membrane Damage, Morphology Change and Rupture by Nonionic Surfactants. *Biophys. J.* **2001**, *81*, 725-736.

54. Partington, J. R.; Hudson, R. F.; Bagnall, K. W. Self-Diffusion of Aliphatic Alcohols. *Nature* **1952**, 169, 583–584.

55. Gumerov, R. A.; Rudov, A. A.; Richtering, W.; Möller, M.; Potemkin, I. I. Amphiphilic Arborescent Copolymers and Microgels: From Unimolecular Micelles in a Selective Solvent to the Stable Monolayers of Variable Density and Nanostructure at a Liquid Interface. *ACS Appl. Mater. Interfaces* **2017**, *9*, 31302-31316.

56. Berezkin, A. V.; Jung, F.; Posselt, D.; Smilgies, D. M.; Papadakis, C. M. Vertical vs Lateral Macrophase Separation in Thin Films of Block Copolymer Mixtures: Computer Simulations and GISAXS Experiments. *ACS Appl. Mater. Interfaces* **2017**, 9, 31291-31301.

57. Suttipong, M.; Grady, B. P.; Striolo, A. Surfactants Adsorption on Crossing Stripes and Steps. *Soft Matter* **2017**, *13*, 862-874.

58. Su, G.; Zhou, X.; Zhou, H.; Li, Y.; Zhang, X.; Liu, Y.; Cao, D.; Yan, B. Size-Dependent Facilitation of Cancer Cell Targeting by Proteins Adsorbed on Nanoparticles. *ACS Appl. Mater. Interfaces*, **2016**, *8*, 30037-30047

59. Liu, Y; Kuksenok, O; He, XM.; Aizenberg, M.; Aizenberg, J.; Balazs, A.C.; Liu, Y.; Harnessing Cooperative Interactions between Thermoresponsive Aptamers and Gels to Trap and Release Nanoparticles. *ACS Appl. Mater. Interfaces* **2016**, *8*, 30475-30483.

60. Suttipong, M.; Grady, B. P.; Striolo, A. Surfactant Aggregates Templated by Lateral Confinement. *J. Phys. Chem. B* **2015**, *119*, 5467-5474.

61. Ge, W. Y.; Li, N. K.; McCormick, R. D.; Lichtenberg, E.; Yingling, Y. G.; Stiff-Roberts, A. D. Emulsion-Based RIR-MAPLE Deposition of Conjugated Polymers: Primary Solvent Effect and Its Implications on Organic Solar Cell Performance. *ACS Appl. Mater. Interfaces* **2016**, *8*, 19494-19506.

62. Lin, S.; Ryu, S.; Tokareva, O.; Gronau, G.; Jacobsen, M. M.; Huang, W.; Rizzo, D. J.; Li, D.; Staii, C.; Pugno, N. M.; Wong, J. Y.; Kaplan, D. L.; Buehler, M. J. Predictive Modelling-Based Design and Experiments for Synthesis and Spinning of Bioinspired Silk Fibres. *Nat. Commun.* **2015**, 6, 6892.

63. Wang, Y; Li, Q.Y.; Liu, X.B.; Zhang, C.Y.; Wu, Z.M.; Guo, X.D., Mesoscale Simulations and Experimental Studies of pH-Sensitive Micelles for Controlled Drug Delivery *ACS Appl. Mater. Interfaces* **2015**, *7*, 25592-25600.

64. Leonforte, F.; Muller, M. Poly(N-isopropylacrylamide)-Based Mixed Brushes: A Computer Simulation Study, *ACS Appl. Mater. Interfaces* **2015**, *7*, 12450-12462.

65. Akhavan, O.; Ghaderi, E.; Akhavan, A. Size-Dependent Genotoxicity of Graphene Nanoplatelets in Human Stem Cells. *Biomaterials* **2012**, *33*, 8017-8025.

66. Liu, S.; Hu, M.; Zeng, T. H.; Wu, R.; Jiang, R.; Wei, J.; Wang, L.; Kong, J.; Chen, Y. Dimension-Dependent Antibacterial Activity of Graphene Oxide Sheets. *Langmuir* **2012**, *28*, 12364-12372.

67. Mu, Q.; Su, G.; Li, L.; Gilbertson, B. O.; Yu, L. H.; Zhang, Q.; Sun, Y.-P.; Yan, B. Size-Dependent Cell Uptake of Protein-Coated Graphene Oxide Nanosheets. *ACS Appl. Mater. Interfaces* **2012**, *4*, 2259-2266.

68. Devaux, P. F.; Herrmann, A.; Ohlwein, N.; Kozlov, M. M. How Lipid Flippases can Modulate Membrane Structure. *Biochim. Biophys. Acta* **2008**, *1778*, 1591-1600.

TOC